JPE 16-3-13

http://dx.doi.org/10.6113/JPE.2016.16.3.946
ISSN(Print): 1598-2092 / ISSN(Online): 2093-4718

A Novel Virtual Space Vector Modulation Strategy for the Neutral-Point Potential Comprehensive Balance of Neutral-Point-Clamped Converters

Chuan-Jin Zhang*, Yi Tang*, Dong Han*, Hui Zhang†, Xiao Zhang*, and Ke Wang*

*,†School of Information and Electrical Engineering, China University of Mining and Technology, Xuzhou, China

Abstract

A novel Virtual Space Vector (VSV) modulation strategy for complete control of potential neutral point (NP) issues is proposed in this paper. The neutral point potential balancing problems of multi-level converters, which include elimination of low frequency oscillations and self-balancing for NP dc unbalance, are investigated first. Then a set of improved virtual space vectors with dynamic adjustment factors are introduced and a multi-objective optimization algorithm which aims to optimize these adjustment factors is presented in this paper. The improved virtual space vectors and the multi-objective optimization algorithm constitute the novel Virtual Space Vector modulation. The proposed novel Virtual Space Vector modulation can simultaneously recover NP dc unbalance and eliminate low frequency oscillations of the neutral point. Experiment results show that the proposed strategy has excellent performance, and that both of the neutral point potential issues can be solved.

Keywords: Low-frequency oscillations, Multi-objective optimization, Neutral point potential unbalance, Self-balancing, Virtual Space Vector

I. INTRODUCTION

Nowadays, the neutral-point-clamped (NPC) three-level converter [1] is an attractive topology for high-power electronic systems due to the high-power density, harmonic performance, and cost savings of its passive components [2]. However, some of the unique pitfalls in three-level NPC converters include the neutral point potential unbalancing issues caused by current flowing to the NP (i_{NP}). These drawbacks consist of two parts, steady-state imbalance and transient-state imbalance [3]. In this paper, the steady-state imbalance caused by component imperfections, transients, imbalanced loads and some other factors is called NP dc unbalance. This unbalance causes a continuous unsymmetrical power flow between the positive and negative dc-links and may destroy the devices. On the other hand, the transient-state imbalance, which is an inherent characteristic of the NPC topology due to the fact that the momentary NP current is not constant, is termed low-frequency oscillation (at three times the fundamental frequency).

At present, there are several methods for NP potential balance control. Some solutions make use of isolated dc-voltage sources or a front-end circuit at the dc side for controlling the NP voltage balance [4]-[7]. There are some other methods that involve improving the modulation algorithm itself to obtain the NP potential balance. Compared with the hardware approaches, the second type does not need extra equipment and reduces the system size [8]. When the voltages on the dc-link capacitors are not kept constant by external DC sources, the modulations must take over the NP voltage balance by themselves [9]. The nearest-three-vector (NTV) method is one of the most commonly used multilevel space vector pulse width modulation (SVPWM) techniques. It has the advantages of a low switching frequency and good output voltage quality [8]. However, the application of the NTV modulation technique in three level NPC converters causes a low frequency oscillation of the NP potential [10], especially systems operating under a high modulation index and a low power factor [2], [11]. To overcome the low frequency oscillation appearing at the NP, the nearest three virtual space vector (NTV^2) modulation method was presented

Manuscript received Sep. 22, 2015; accepted Jan. 5, 2016.
Recommended for publication by Associate Editor Honnyong Cha.
†Corresponding Author: zhanghuicumt@126.com
Tel: +86-15996956902, China University of Mining and Technology
*School of Information and Electrical Engineering, China University of Mining and Technology, China

in [10]. It can eliminate low frequency oscillations over the full range of the converter output voltage and for all of the load power factors. However, it does not have enough self-balancing capability to restore the NP dc unbalance under most conditions. Therefore, the NP dc unbalance caused by the different initial conditions of the voltages on dc-link capacitors or any other reason (dead times, asymmetric values of the components, etc.), can no longer recover by itself [9]. Several papers have referred to NP self-balancing [2], [3], [12]. However, the self-balancing mechanism of NTV^2 modulation is different from that of NTV modulation, and the self-balancing mechanism of NTV^2 has never been analyzed. Considering the defect of NTV^2 modulation, an improved virtual vector with a control loop was proposed in [9]. Although it introduces two distribution variables, there are still uncontrolled areas in the space vector plane. In [14], a similar solution for NTV^2 modulation has the same flaws as [9]. An optimized NTV^2 (ONTV^2) PWM with closed-loop control [15] can also comprehensively achieve this objective. However, the design of the closed-loop control scheme interfacing the ONTV^2 PWM is not straight forward and this type of compensators does not take into account the instantaneous values of the output currents [16]. A double-signal pulse width modulation (DSPWM) based on carrier-based modulation using two modulation signals per phase was proposed in [15]. The DSPWM has the same effect as the NTV^2. It can completely eliminate low-frequency oscillations of the NP potential. However, it does not provide a self-balancing that is strong enough to recover the NP dc unbalance. Therefore, a compensation loop was added to the DSPWM in [16]. The offset applied to the modulation signals must be proper or it will make the NP dc unbalance even worse.

In this paper, the mechanism of the self-balancing of NTV^2 modulation is analyzed in detail. Then a switch model of the self-balancing mechanism is developed. From this model it can be seen that the NPC converter applied with NTV^2 modulation only has the self-balancing characteristic under a pure resistance load, and hardly recoveries the NP dc unbalance without external active controls. To overcome this drawback and to improve the ability of restoring the NP dc unbalance in a converter using NTV^2 modulation, this paper proposes a set of improved virtual space vectors and a multi-objective optimization algorithm. The improved virtual space vectors eliminate the uncontrolled areas in [9] and put the whole SV plane under control without increasing the algorithm complexity.

The remainder of this paper is organized as follows. Section II describes the NTV and NTV^2 modulation strategies. Section III discusses the mechanism of self-balancing under both the NTV^2 and NTV modulations. Section IV presents the novel virtual space vectors and a multi-objective optimization algorithm for recovering the NP dc unbalance in NTV^2 modulation. Section V shows some experiment results to validate the improved virtual space vectors and the proposed multi-objective optimization scheme. Finally, Section VI outlines some conclusions.

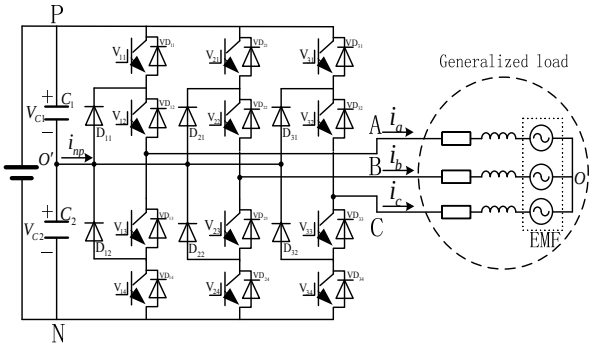

Fig. 1. Circuit of a NPC three-level converter.

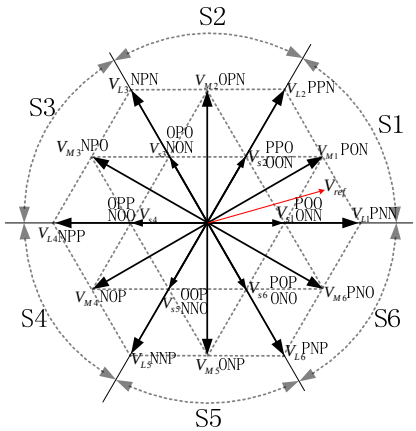

Fig. 2. Space vector diagram of NPC three-level converter and the symmetry sectors.

II. NTV AND NTV^2 MODULATION

A typical NPC three-level converter is shown in Fig. 1. With the variety change of the back electromotive force (EMF), four quadrant operations can be realized in the NPC three-level converter [16]:

A space vector diagram of a three-level converter with all of the switching state combinations [17] is shown in Fig. 2.

According to the magnitude of the three-level voltage vectors, these space vectors can be divided into four categories: zero vectors V_Z; small vectors V_{Sx}; large vectors V_{Lx} and medium vectors V_{Mx}, where x=1,2,3,…,6. Due to the circular symmetry of the three-phase system, the space vector plane is divided into six sectors as shown in Fig. 2. However, taking first sector into account is sufficient. Table I presents the four vector types of the first sector (S1) of a NPC converter.

Among these four types, only the medium and small vectors connect the phase current to the NP. These two types of vectors influence the NP potential balance as they charge or discharge the dc-link capacitors [11].

A. NTV Pulse Width Modulation

TABLE I
VECTOR TYPES OF THE FIRST SECTOR

Vector Type	Voltage Vector	NP Current
small	V_{ONN},V_{POO}	$\pm i_a$
large	V_{PNN},V_{PPN}	0
middle	V_{PON}	i_b
small	V_{PPO},V_{OON}	$\pm i_c$
zero	V_{OOO},V_{PPP},V_{NNN}	0

For the sake of convenience, a reference voltage space vector V_{ref} is introduced and the first sector is subdivided into four smaller triangles (refer to Fig. 2). In the conventional SVPWM, the first step is to determine the location of V_{ref} and to find the nearest three vectors. The next step involves the calculation of the duty cycle of selected vectors with trigonometric functions and the volt-second balance principle. At last, an optimized vector sequence (seven-segment pattern) [19], which can reduce the switching loss and distortion rate at the AC terminal, is used to compose the reference vector. The reference vector can be obtained from Equ. (1).

$$V_{ref} = \frac{\frac{t_1}{2}}{T_s}V_{POO} + \frac{t_2}{T_s}V_{PNN} + \frac{t_3}{T_s}V_{PON} + \frac{\frac{t_1}{2}}{T_s}V_{ONN} \quad (1)$$

However, the application of NTV modulation causes a low frequency oscillation of the NP potential in a three-level NPC converter, especially in systems under the condition of high modulation indexes and a low-power-factor [2].

B. NTV^2 Pulse Width Modulation

To overcome the drawbacks of the NTV PWM and to achieve full control of the neutral-point voltage, a novel scheme referred to as virtual space vector PWM was presented in [10] and further developed in [8], [9], [13], [15], [16], [25]. The virtual space vector is a linear combination of basic space vectors as shown in Fig. 2. The design principle of the desired virtual vectors is ensuring that the average neutral point current is equal to zero during its dwell time. To get the virtual space vectors, it is assumed that the value of the three-phase current is fixed during an entire sampling period since the sampling frequency is much higher than the constant supply frequencies of the source.

1) Virtual Middle Vectors: Taking the middle vector V_{PON} located in the first sector as an example, when V_{PON} is used for synthesizing the reference voltage vector, the current flowing into NP is equal to $i_b(t)$. Since the current is not equal to zero in most cases, this leads to an offset of the NP potential. In order to compensate the effects of $i_b(t)$, the specific small vectors V_{ONN} and V_{PPO} are added to compose the virtual middle vector of S1(V_{VM1}) during the duration of t_{PON} (the dwell time of V_{PON}). Furthermore, t_{PON} should be divided equally for the above three vectors. The virtual middle vector of S1 is defined as Equ. (2).

$$V_{VM1} = \frac{1}{3}(V_{PON} + V_{PPO} + V_{ONN}) \quad (2)$$

In a three-phase system without a midline, the sum of the three-phase current is zero at any moment. As a result, the average NP current is zero since $i_{NP} = \frac{1}{3}(i_a + i_b + i_c) = 0$ during the dwell time of V_{VM1}.

2) Virtual Small Vectors: Each small vector has two different switching states which are called redundancy vectors. The pair of redundancy vectors produces an identical output voltage at the AC terminal. However, their effect on the natural point is opposite in the same sampling period. Virtual small vectors are obtained from an equitable combination of redundancy vectors as Equ. (3).

$$V_{VS1} = \frac{1}{2}(V_{POO} + V_{ONN}), V_{VS2} = \frac{1}{2}(V_{PPO} + V_{OON}) \quad (3)$$

3) Virtual Large Vectors: Because the NP current of the large vectors is zero, the virtual large vectors are obtained directly from basic large vectors as Equ. (4).

$$V_{VL1} = V_{PNN}, V_{VL2} = V_{PPN} \quad (4)$$

4) Virtual Zero Vectors: Virtual zero vectors can be defined by Equ. (5).

$$V_{VZ} = V_{NNN} \text{ or } V_{OOO} \text{ or } V_{PPP} \quad (5)$$

The basic zero vectors do not have any effect on the NP potential. Therefore, the virtual vectors do not need to make any changes to them. However, in order to reduce the dynamic loss and switch stress, the specific vector of the three zero vectors should be chosen to get a smooth transition of the switching state.

All of the virtual vectors of S1 ($V_{VS1,2}$, V_{VM1}, $V_{VL1,2}$, V_{VZ}) are shown in Fig. 3(a), and in Fig. 3(b) the first sector of the virtual space vector diagram is divided into five parts [10] for positioning the reference vector. Like NTV modulation, NTV^2 modulation has three similar steps in the synthesis of the reference vector. Firstly, the specific nearest three virtual vectors should be found. Secondly, the duty cycle of the selected virtual vectors is calculated by the volt-second balance principle. Finally, an appropriate vector sequence is applied to complete the voltage output. The reference vector under NTV^2 modulation can be obtained from Equ. (6).

$$\begin{aligned} V_{ref} &= \frac{t_{VS1}}{T_s}V_{VS1} + \frac{t_{VM1}}{T_s}V_{VM1} + \frac{t_{VL1}}{T_s}V_{VL1} \\ &= \left(\frac{\frac{t_{VS1}}{2} + \frac{t_{VM1}}{3}}{T_S}\right)V_{ONN} + \frac{t_{VL1}}{T_s}V_{PNN} + \frac{t_{VM1}}{3T_S}V_{PON} \\ &\quad + \frac{t_{VS1}}{2T_S}V_{POO} + \frac{t_{VM1}}{3T_S}V_{PPO} \end{aligned} \quad (6)$$

Because the average NP current is equal to zero in the duty cycle of the corresponding virtual vector, NTV^2 modulation techniques eliminate the low frequency oscillations of the NP potential in NPC converters. However, NTV^2 modulation cannot restore the NP dc unbalance without additional control. The self-balancing of the NP dc unbalance in NTV and NTV^2 modulation will be explored in detail in section III.

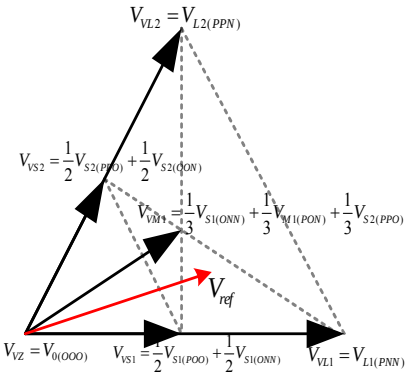

(a) Virtual vectors of first sextant.

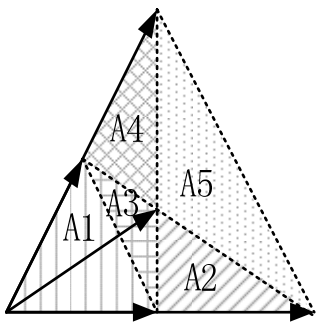

(b) Areas for nearest three virtual vectors.

Fig. 3. Virtual vectors.

III. MECHANISM OF SELF-BALANCING

For the NP dc unbalance, the NP potential may be "self-balanced," even without any active controls [2]. This self-balanced mechanism has been verified in [3], and the effectiveness is related to the modulation technique, the harmonics of the switching functions and the load impedance. In [3], [12] analyses of the natural balancing theory are established in the frequency domain. However, the relationship among the voltage space vectors, the NP current and the balance mechanism is fuzzy based on the conclusions gained from [3], [12]. In this paper, an analysis of the self-balancing mechanism will be fulfilled in the time domain. Moreover, the inner relationship among the three elements (voltage space vectors, NP current and self-balancing mechanism) is established. Due to the circular symmetry, only sector 1 is considered in detail. The following variables, which describe the unbalance in the dc capacitor voltages, are defined as Equ. (7).

$$\begin{cases} U=\frac{1}{2}(U_{C1}+U_{C2}) \\ \delta=\frac{1}{2}(U_{C1}-U_{C2}) \end{cases} \tag{7}$$

Furthermore, some assumptions about the unbalance parameters should be made: a) the variation of δ is slow compared to the dynamics of the rest of the system; b) δ is a dc voltage and the system is in the steady state. Therefore, the amplitude and phase of the basic space vectors in S1 will change as shown in Equ. (8).

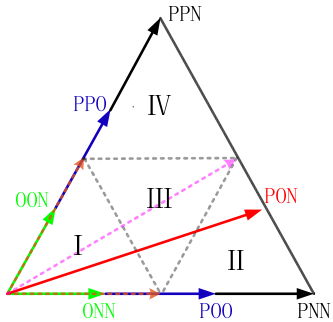

Fig. 4. Amplitude and phase of vectors in S1 as NP unbalanced.

$$\begin{cases} V_{ONN}^{*}=(U-\delta)e^{j0}=V_{ONN}-\delta e^{j0}, V_{POO}^{*}=(U+\delta)e^{j0}=V_{POO}+\delta e^{j0} \\ V_{OON}^{*}=(U-\delta)e^{j\frac{\pi}{3}}=V_{OON}-\delta e^{j\frac{\pi}{3}}, V_{PPO}^{*}=(U+\delta)e^{j\frac{\pi}{3}}=V_{PPO}+\delta e^{j\frac{\pi}{3}} \\ V_{PON}^{*}=V_{OON}^{*}+V_{POO}^{*}=(U-\delta)e^{j\frac{\pi}{3}}+(U+\delta)e^{j0}=V_{PON}+\delta e^{-j\frac{\pi}{3}} \\ V_{PNN}^{*}=V_{PNN}, V_{PPN}^{*}=V_{PPN} \end{cases} \tag{8}$$

Here, the ideal basic vectors under the NP balanced state are expressed without *. On the other hand, the ones with * represent the actual basic vectors under the NP unbalanced state. When $\delta>0$, the basic vectors of S1 are shown in Fig. 4.

A. Self-Balancing of NTV Modulation

If the NP is perfectly balanced, the expected voltage space vector V_{ref} appears at the ac terminal. However, when $\delta\neq 0$ in Equ. (9), there is a voltage deviation vector between the ideal reference voltage vector and the actual output voltage vector. Unbalanced factors and basic vector deviation are not considered in the dwell time calculation of the selected basic vectors. For example, substituting Equ. (8) into Equ. (1), the real composed vector is obtained under the NP dc unbalanced state as follows:

$$\begin{aligned} V_{ref} &= \frac{\frac{t_1}{2}}{T_S}(V_{POO}+\delta e^{j0})+\frac{t_2}{T_S}V_{PNN} \\ &\quad +\frac{t_3}{T_S}(V_{PON}+\delta e^{-j\frac{\pi}{3}})+\frac{\frac{t_1}{2}}{T_S}(V_{ONN}-\delta e^{j0}) \\ &= V_{ref}^{*}+\frac{t_3}{T_S}\delta e^{-j\frac{\pi}{3}} \end{aligned} \tag{9}$$

Equ. (9) refers to the voltage deviation vector of the introduced reference vector shown in Fig. 2. The dwell time of this deviation vector is t_3, the amplitude is $\frac{t_3}{T_S}\delta$, and the phase is $-\frac{\pi}{3}$. There must be a current deviation vector under the action of the corresponding voltage deviation vector for the duration of t_3. With a change of the load, the phase of the current deviation vector is also changed, and the range of the current deviation vector's phase is $-\frac{5}{6}\pi\sim\frac{1}{6}\pi$. The voltage

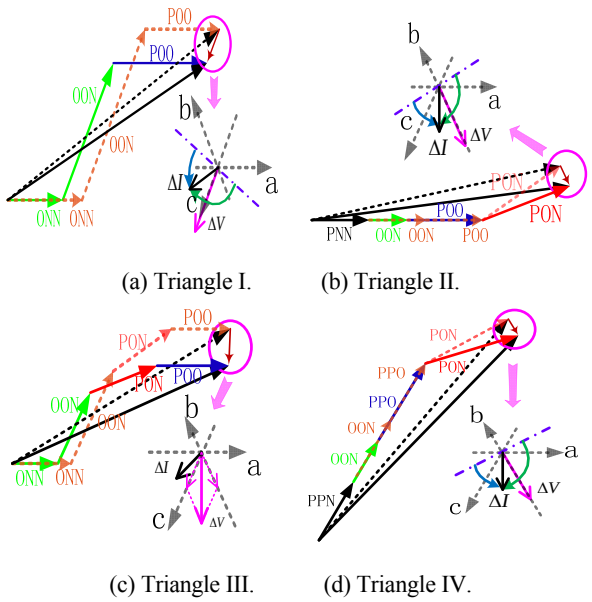

Fig. 5. Voltage and current deviation vectors in S1.

deviation vector of V_{ref}, the current deviation vector of V_{ref} and its phase scope are shown in Fig. 5(b). On the other hand, the NP current is equal to i_b during the dwell time of ΔV (t_3) and the projection component of ΔI in the B axis is below zero. In this case the current deviation vector discharges the upper capacitor and charges the lower capacitor. As a result, the NP potential of the system tends to be balanced.

The conclusion is obtained from analyzing triangle II, and can also be obtained by studying the other triangles. Figs. 5(a)-(d) describe the deviation vectors in all four of the triangles of S1.

In Figs. 5(a)-(d), the dotted lines represent the ideal voltage vectors without the NP dc unbalance and the solid lines represent the actual voltage vectors obtained in the dc unbalanced state. In order to facilitate the analysis, the vector sequence of the reference vectors in triangle II and IV have been made to change. This change does not have any impact on the final synthesis of the reference vector.

The above conclusion is obtained from an analysis of a typical load, shown in Fig. 5(b), under the state of $\delta > 0$. However, it is universally applicable when $\delta < 0$. From Equ. (9), the actual output voltage vector can be split into two parts. The ideal part maintains the normal operation of the system and the deviation part is regarded as a disturbance which makes the NP potential self-balance in NTV modulation under the dc unbalanced state.

B. Self-Balancing of NTV² Modulation

The analysis method of self-balancing based on the deviation vector is more intuitive than the method based on the frequency-domain in [3], [12]. However, the amplitude and phase of the virtual space vectors will not be influenced, when the NP dc unbalance appears. The new virtual space vectors of

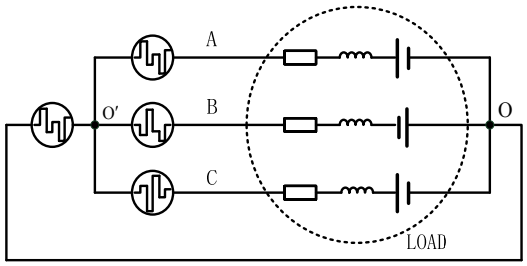

Fig. 6. Equivalent model of NPC converter during one sampling period.

S1 are represented as Equ. (10).

$$\begin{cases} V_{VS1}^{*} = \frac{1}{2}(V_{POO} + \delta e^{j0} + V_{ONN} - \delta e^{j0}) = V_{VS1} \\ V_{VS2}^{*} = \frac{1}{2}(V_{PPO} + \delta e^{j\frac{\pi}{3}} + V_{OON} - \delta e^{j\frac{\pi}{3}}) = V_{VS2} \\ V_{VM1}^{*} = \frac{1}{3}(V_{PPO} + \delta e^{j\frac{\pi}{3}} + V_{ONN} - \delta e^{j0} + V_{PON} \\ \qquad + \delta e^{-j\frac{\pi}{3}}) = V_{VM1} \\ V_{VL1}^{*} = V_{VL1}, V_{VL2}^{*} = V_{VL2} \end{cases} \tag{10}$$

In Equ. (10), there are no deviation vectors which makes the NPC converter using NTV² modulation have self-balancing capability under the NP dc unbalanced state. As discussed in [14], NTV² PWM does not belong to modulations with the property of naturally recovering the dc-link voltage balance after a perturbation. However, this conclusion is not completely correct. The self-balancing analysis of NTV modulation is based on a steady state model and this method takes the synthetic vector as a whole within one sampling period without considering the dynamic effects of the switching transient state.

In this paper, a dynamic switch model based on the process of switching is built for studying the self-balancing mechanisms of NTV² modulation. In one sampling period, the NPC three-level converter system shown in Fig. 1 can be simplified as the circuit in Fig. 6. Here, the phase voltage $u_{XO'}$ (X=A, B, C) and the common mode voltage $u_{OO'}$ are represented by the pulse power.

Expression of the common mode voltage can be obtained from Fig. 1 [17].

$$u_{OO'} = \frac{1}{3}(\sum_{X} u_{XO'} - u_{XO}), (X = A, B, C) \tag{11}$$

Because of the symmetry of the NPC converter and three-phase load the sum voltage of the three-phase load is zero. Then Equ. (11) can be rewritten as $u_{OO'} = \frac{1}{3}\sum_{X} u_{XO'} (X = A, B, C)$. The dwell time and switching sequences of the reference vector can be acquired by solving Equ. (6). Then they should be put into Equ. (11) to obtain u_{XO}, $u_{XO'}$, and $u_{OO'}$ (X=A, B, C). All of which are shown in Fig. 7.

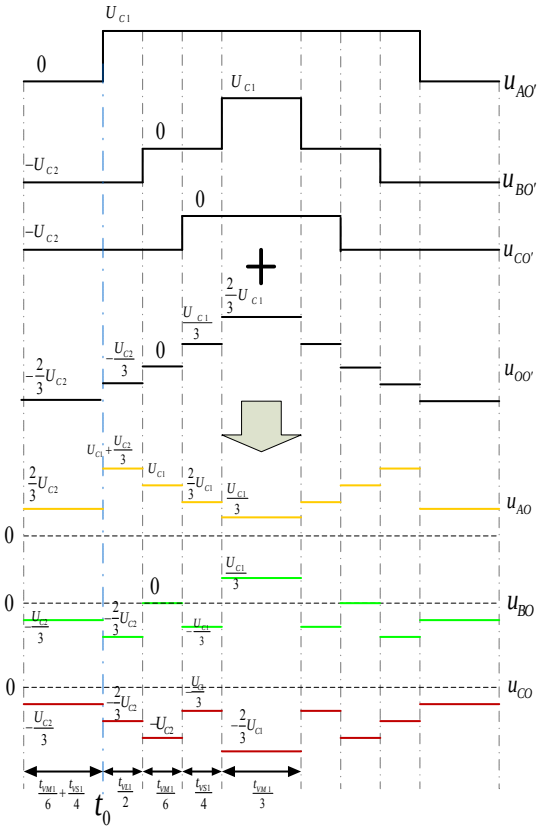

Fig. 7. Three-phases voltage of the NPC three-level system.

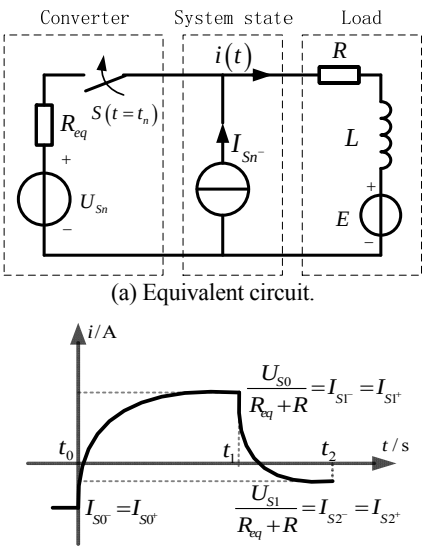

(a) Equivalent circuit.

(b) Response curve.

Fig. 8. Switch model of NPC converter at the switching state changing instant.

At the moment of t_0, the switching state is changing from ONN to PNN and all of the three-phase load voltages jump at the same time. Similar steps of the load phase voltage will happen at the time of each switching state change (t_n) beside t_0. Therefore, the switch model of the NPC converter at t_n may be depicted as a first-order full response circuit, as shown in Fig. 8(a).

In Fig. 8 the current source I_{Sn^-} indicates the steady-state load current the moment t_n before the switching state changes, and due to the resistive–inductive load, the system current mutation does not occur. Thus, $I_{Sn^-}=I_{Sn^+}$; the voltage source U_{Sn} and the switch S compose the step excitation source; R_{eq} is the equivalent internal resistance of the step source and $R+jwL$ is the load equivalent impedance; and the counter electromotive force is replaced by a DC voltage source E when the converter working as an inverter EMF is equal to zero. The circuit model shown in Fig. 8 is easy solve by the three element method, as in Equ. (12).

$$\begin{aligned} i(t) &= i(\infty)+[i(0_+)-i(\infty)]e^{-\frac{t}{\tau}} \\ &= \frac{U_S}{R_{eq}+R}+[I_S-\frac{U_S}{R_{eq}+R}]e^{-\frac{t}{L}(Req+R)} \end{aligned} \tag{12}$$

Here, $\tau=\frac{L}{R_{eq}+R}$ is the time constant of the circuit. Due to the fact that $R_{eq}<<R$, the time constant can be reduced as $\tau\approx\frac{L}{R}$. The time constant τ is only decided by the load characteristics. It has nothing to do with the external exciting source or the initial state of the circuit. The transition process of the circuit finishes after a time slot of $3\tau\sim5\tau$ in engineering. To obtain the theoretical maximum time constant, which makes the circuit into the steady-state between the two switching states, it is assumed that the switching state has only one transformation in half of a sampling period (V_{ref} is just located in the position of V_{VS1}). This should satisfy $3\tau\le\frac{T_S}{2}$ as a result $\tau_{\max}=\frac{T_S}{6}$. In this condition, it is easy to get the system power factor as $\cos\varphi=\frac{R}{\sqrt{R^2+L^2}}=\frac{1}{\sqrt{1+(\frac{L}{R})^2}}=\frac{1}{\sqrt{1+\tau^2}}$. If $\tau\le\tau_{\max}=\frac{T_S}{6}$, then $\cos\varphi\ge\frac{6}{\sqrt{36+T_S^2}}$, and there will be enough time to make sure the system enters the steady-state before the next switching state jump. First the most special circumstances of the converter working in the unity-power factor state is discussed. This means that the load is pure resistance and τ=0. As a result, the circuit immediately enters the steady state at the instant of the switching state jump. When $\delta>0$ and $\cos\varphi=1$, it is possible to can get the NP current under the corresponding voltage vector as shown in Table Ⅱ.

The accumulation of the NP potential deviation in one sampling period is $-\frac{2}{3}\frac{\delta}{R}(t_{VS1}+t_{VM1})$ and its value is less than zero. The voltage of C_1 decreases and voltage of C_2 increases. As a result the NP potential tends to balance by itself

TABLE II
NP CURRENT UNDER CORRESPONDING VOLTAGE VECTOR IN DC UNBALANCE STATE

Operating Vectors	Dwell Time	Value of NP Current	Deviation of NP Potential
V_{ONN}	$\frac{1}{2}t_{VS1}+\frac{1}{3}t_{VM1}$	$\frac{2}{3}\frac{U-\delta}{R}$	$\frac{2U-\delta}{3R}(\frac{1}{2}t_{VS1}+\frac{1}{3}t_{VM1})$
V_{PNN}	t_{VL1}	0	0
V_{PON}	$\frac{1}{3}t_{VM1}$	$-\frac{2}{3}\delta$	$-\frac{2}{3}\delta(\frac{1}{3}t_{VM1})$
V_{POO}	$\frac{1}{2}t_{VS1}$	$-\frac{2}{3}\frac{U+\delta}{R}$	$-\frac{2}{3}\frac{U+\delta}{R}\frac{1}{2}t_{VS1}$
V_{PPO}	$\frac{1}{3}t_{VM1}$	$-\frac{2}{3}\frac{U+\delta}{R}$	$-\frac{2}{3}\frac{U+\delta}{R}\frac{1}{3}t_{VM1}$

in this case. The entire switching states of the reference vector and the accumulated deviation of the NP potential in one sampling period are shown in Fig. 9(a).

It is necessary to discuss the much more general case of a resistive–inductive load. If the power factor of a system meets the following condition $\cos\varphi \geq \frac{6}{\sqrt{36+T_S^2}}$, the duration of one vector will be enough to ensure the load current entering the steady-state. The switching process of this case is shown in Fig. 9(b). Compared with a pure resistive load, the current response of the resistive-inductive load has one more approaching process, which influences the accumulation of the NP potential deviation in one sampling period. When considering the approaching process of the load currents, the accumulation of the NP potential deviation in one sampling becomes as follows:

$$\Delta V = \frac{2}{3}\frac{\delta}{R}(t_{VS1}+t_{VM1})(e^{-\frac{R}{L}t}-1) \quad (13)$$

With the power factor of the system increasing, the value of ΔV gets closer and closer to zero. This means that the ability to restore the dc unbalance by itself under NTV^2 modulation is gradually getting worse and worse. This conclusion can be described intuitively in Fig. 9.

When $\tau > 10\tau_{max}$ ($\cos\varphi \leq 0.985$) it is deemed that the load current in one sampling period is not changed, and that it can be seen as a constant as shown in Fig. 9(d). In this condition, the dc unbalanced voltage will not be restored by itself since the average NP current is equal to zero. The three-level NPC converter under NTV^2 modulation hardly has the self-balancing characteristic, unless it was employed with a pure resistance load.

C. Comparison of Self-Balancing Capability Based on NTV and NTV^2 Modulation

As it can be seen from the simulation results shown in Fig. 10, three-level converters using the above two types of modulation both have the NP potential self-balancing

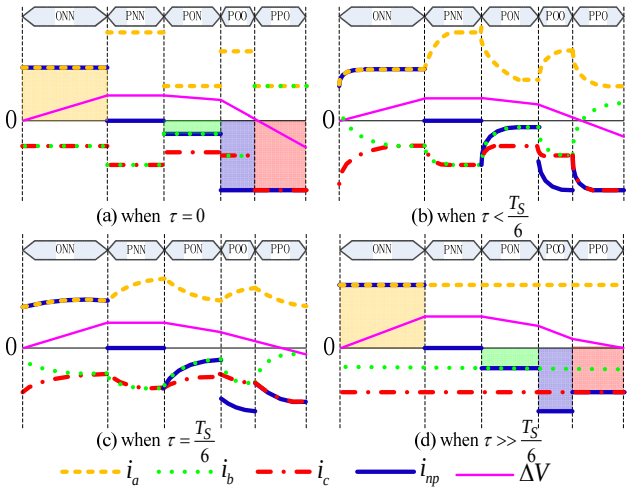

Fig. 9. Accumulation of NP voltage deviation with NTV^2 modulation under typical load.

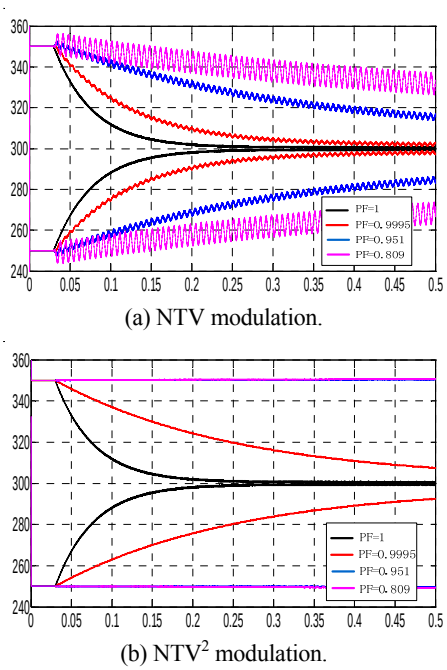

(a) NTV modulation.

(b) NTV^2 modulation.

Fig. 10. Process of self-balancing when NP potential unbalanced.

characteristic. However, this self-balancing capability is reduced sequentially with a decrease of the power factor in NTV^2 modulation. In fact, the dc unbalance will never be recovered when PF ≤ 0.951 without extra control. Moreover, with a decrease of the power factor there is an obvious low frequency oscillation in the NP potential under NTV modulation. It is necessary to strengthen the capacity of the suppression of the NP dc unbalance in NTV^2 modulation.

IV. IMPROVED VIRTUAL VECTORS AND MULTIPLE OBJECTIVE OPTIMIZATION ALGORITHM

From the above analysis, although the self-balancing ability of NTV modulation is much stronger than that of NTV^2, balancing the capacitor voltage of NPC converters in the steady

state has been a burning issue and a great deal of research has addressed this problem [20]-[22].

A. Uncontrolled Area of the NP dc Unbalance and Improved Virtual Vectors

A well-known strategy has been introduced to solve this problem by manipulating the redundant switching vectors (a couple of small vectors) in NTV modulation [3], [23], [24]. A similar strategy, which made use of the non-equal shared dwell time between a couple of redundant vectors to reconstruct the small virtual vectors [9], was applied in NTV^2 modulation to overcome the NP potential dc unbalance in NPC converters. In [10], the proportion of any redundant vector in a virtual small vector is fifty percent as shown in Equ. (3). As a result, the dwell time of the two pairs of redundant vectors used to form V_{VS1} and V_{VS2} is generated by $d_{ONN}=\frac{1}{2}d_{VS1}, d_{POO}=\frac{1}{2}d_{VS1}$ and $d_{OON}=\frac{1}{2}d_{VS2}, d_{PPO}=\frac{1}{2}d_{VS2}$. When the method proposed in [9] is applied in NTV^2 modulation to restrain dc unbalance, the distribution ratio of the dwell time of the corresponding redundant vectors will be changed by modifying the variables x_1 and x_2, which are as follows $d_{ONN}=\frac{1-x_1}{2}d_{VS1}, d_{POO}=\frac{1+x_1}{2}d_{VS1}$, $d_{OON}=\frac{1-x_2}{2}d_{VS1}, d_{PPO}=\frac{1+x_2}{2}d_{VS1}$ and $x_1, x_2 \in [-1,1]$. With the parameters x_1 and x_2 changing, the average NP current is not zero during the dwell time of V_{VS1} and V_{VS2}. Thus, the NP potential dc unbalance can be recovered by adjusting the parameters x_1 and x_2. On the other hand, no matter what changes are made in the values of x_1 and x_2, the phase, amplitude and duty cycle of V_{VS1} and V_{VS2} always stay the same. Therefore, the reference vector is not affected. However, there must be virtual small vectors as the selected nearest vectors in this strategy. Otherwise the average NP current is zero in one sampling period, and the NP potential dc unbalance exists continuously.

For the NTV^2 modulation described in Section II, in order to facilitate the selection of the specific three vectors closest to the reference vector, each sector is subdivided into five regions as shown in Fig. 3. If the reference vector is located in A5 of S1, the selected nearest three virtual vectors for synthesizing the reference vector are V_{VL1}, V_{VL2} and V_{VM1}. There is no virtual small vector as the selected vector in this region. Therefore, the method proposed in [9] does not work in A5. In this paper, all of the A5 regions of sectors 1 to 6 are called the uncontrolled areas of the NP dc unbalance under the conventional NTV^2 modulation, as shown in Fig. 11. The size of the uncontrolled areas is a function of the modulation index and it can be represented by an angle. According to the trigonometric theorem, it is possible to obtain the formula of the uncontrolled area as Equ. (14). Here, M represents modulation index.

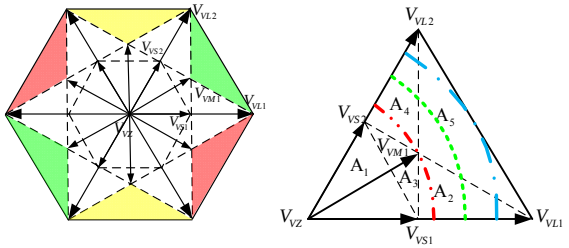

(a) Uncontrolled area in SV plane. (b) Uncontrolled area in S1.

Fig. 11. Uncontrolled area of NP dc unbalance under conventional NTV^2 modulation.

$$A_{disc}\% = \frac{6\arcsin(\frac{5}{6}\pi - \frac{\sqrt{3}}{3M})}{\pi} \tag{14}$$

In Fig. 11(b), with the incensement of the modulation index, the size of the uncontrolled area increases gradually, and several key conclusions are as follows: a) when M>2/3 the uncontrolled area begin appearing (represented by the red dotted line); b) when M=0.8165 the uncontrolled area is at 50% (represented by the green dotted line); c) when M=1 the area is more than 82.5% (represented by the blue dotted line).

The nearest three vectors without adjustable parameters and a fixed proportion of basic vectors in the virtual vector are major causes of the uncontrolled areas in all of the A5 regions. An algorithm for the optimized virtual vector (ONTV^2) with a dynamic adjustment coefficient was first presented in [25]. However, the primary target of the ONTV^2 is to decrease the distortion rate at the AC terminal, and it does not take into account the NTV^2 without the self-balancing ability to recover the NP dc unbalance. In the meantime a coefficient without appropriate constraints, which leads to final generated virtual vectors and division of the SV plane distortion, sharply increases the algorithm complexity of the ONTV^2. A closed-loop control scheme interfacing the ONTV^2 [14] enhances the capacity of suppressing the NP dc unbalance. However, the offset adding to ONTV^2 has similar defects as the strategies in [15], [16], which needs some additional constraints for compensation. Otherwise, it cannot eliminate the dc unbalance, but aggravate it further.

In this paper, a set of improved virtual vectors are proposed to achieve NP dc balancing for all of the regions. The improved virtual vectors of S1 are shown in Equ. (15).

$$\begin{cases} V_{VM1}=\frac{1+K_M}{3}V_{PON}+\frac{1-K_M}{3}(V_{PPO}+V_{ONN}) \\ V_{VS1}=\frac{1-K_{S1}}{2}V_{POO}+\frac{1+K_{S1}}{2}V_{ONN} \\ V_{VS2}=\frac{1-K_{S2}}{2}V_{PPO}+\frac{1+K_{S2}}{2}V_{OON} \\ V_{VL1}=V_{PNN}, V_{VL2}=V_{PPN} \\ V_{VZ}=V_{NNN}\ or\ V_{OOO}\ or\ V_{PPP} \end{cases} \tag{15}$$

Unlike the traditional virtual vectors, the improved virtual vectors contain three additional variable parameters which are K_M, K_{S1} and K_{S2}. In Equ. (15), the middle virtual vector can

TABLE III
NP CONTROL FACTOR IN EACH REGION OF S1

Region	Virtual Vectors	Adjustment Factor	NP Current
A1	V_{VS1}, V_{V0}, V_{VS2}	K_{S1}, K_{S2}	$\pm i_a, \pm i_c$
A2	$V_{VS1}, V_{VM1}, V_{VL1}$	K_{S1}, K_{M1}	$\pm i_a, \pm i_b$
A3	$V_{VS1}, V_{VM1}, V_{VS2}$	K_{S1}, K_{M1}, K_{S2}	$\pm i_a, \pm i_b, \pm i_c$
A4	$V_{VS2}, V_{VM1}, V_{VL2}$	K_{S2}, K_{M1}	$\pm i_b, \pm i_c$
A5	$V_{VL1}, V_{VM1}, V_{VL2}$	K_{M1}	$\pm i_b$

dynamically distribute the duty cycle with the adjustment factor K_M in addition to the two small virtual vectors. The roles of K_{S1} and K_{S2} are identical with those of x_1 and x_2 referred to in [9]. On the other hand, the design process and working principle of x_1 and x_2 have been studied in the above paper. Consequently, only the newly introduced balance parameter K_M will be discussed in detail.

Considering the increasing complexity of the algorithm caused by the adjustment coefficient presented in [25], when introducing a regulatory factor of the middle virtual vector (K_M) the original middle virtual vector is split into two parts: $V_{VM11}=\frac{1-K_M}{3}V_{PON}$ and $V_{VM12}=\frac{1+K_M}{3}(V_{PPO}+V_{ONN})$, where $-1\le K_M\le 1$. As a result, when K_M changes, the amplitude and phase of the new middle virtual vector remain unchanged. Therefore, the dwell times of the corresponding virtual vectors calculated by the voltage second balance principle are still available and do not need to be modified. This ensures that the proposed improved virtual vectors do not introduce additional computations.

When $V_{VM11}=\frac{1-K_M}{3}V_{PON}$ is active, the phase B current i_b flows into the NP and influences the NP potential. On the other hand, when $V_{VM12}=\frac{1+K_M}{3}(V_{PPO}+V_{ONN})$ is active, -i_b influences the NP potential. Therefore, according to the direction of the phase B current, the NP potential can be effectively controlled by adjusting K_M. On the other hand, when the reference vector falls within the A5 regions, there must be one virtual middle vector among the selected nearest vectors. As a result, the proposed improved virtual vectors can eliminate the uncontrolled areas of the dc unbalance in NTV^2 modulation. Table III describes the distribution of the NP control factors in each region of S1.

A set of suitable adjustment factors obtains a good performance of the NP dc unbalance recovery process. This paper provides a multi-objective optimization algorithm to calculate the appropriate values of the factors.

B. Multi-objective Optimization Algorithm

The circuit of the NPC converter dc side in Fig.1 can be simplified as shown in Fig. 12.

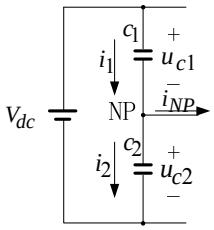

Fig. 12. Simplified model of NPC converter dc side.

Assuming that the two dc-link capacitors have the same value, the currents i_1 and i_2 can be described by the following expressions [15].

$$\begin{cases} i_1 = C_1\dfrac{du_{C1}}{dt} \\ i_2 = C_2\dfrac{du_{C2}}{dt} \\ i_{NP} = i_1 + i_2 \end{cases} \tag{16}$$

In Equ. (16), taking the first and second formulas into the third one will get $v_{NP}=\frac{1}{C}\int_0^t i_{NP}(t)dt+v_{NP0}$, where $v_{NP}=u_{C1}-u_{C2}$ and v_{NP0} is the NP potential at initial time. In a digital system the integral calculation is usually discredited. Therefore, the NP potential can be expressed as Equ. (17).

$$v_{NP}(k)=\frac{1}{C}\sum_{k=1}^{N} i_{NP}(k)T_S+v_{NP0} \tag{17}$$

Where, T_s is the sampling period, and the product of the NP current and time are called the basic elements which affect the change trend of the NP potential. In NTV^2 modulation the reference vector is composed by the nearest three virtual vectors, and the NP current changes with the switching of the space vectors. At a certain switching state, the NP current may be one of the three-phase load currents or the sum of any two phase load currents as shown in Fig.9. A much more general form of the basic elements in any sampling period can be described by the linear combination of the product between the ABC three-phase currents and the dwell time, which can be deduced in Equ. (18).

$$v_{NP}(k)=\frac{1}{C}\sum_{k=1}^{N}\sum_{m=a,b,c} i_m(k)\cdot t_{m0}(k)+v_{NP0} \tag{18}$$

From Equ. (18) it is not difficult to see that changing the sign and numerical value of the basic element controls the NP potential flexibly. On the other hand, the change rate of the NP potential is another significant index which is used for evaluating the NP control strategy and it can be expressed by the difference of the NP potential between the adjacent two sampling periods. The expression of the NP potential change rate is shown as Equ. (19).

$$\begin{aligned}\Delta v_{NP}(k) &= v_{NP}(k)-v_{NP}(k-1) \\ &= \frac{1}{C}\sum_{m=a,b,c} i_m(k)\cdot t_{m0}(k)\end{aligned} \tag{19}$$

When a reference vector located in S1 is synthesized by the improved virtual vectors proposed in the previous section, a concrete manifestation of the NP potential change rate is obtained by taking Equ. (15) into (19) as follows.

$$\begin{aligned}\Delta v_{NP}(k) &= \frac{2}{C} i_a(K)\cdot t_{VS1}(K)\cdot K_{S1}(K) \\ &+ \frac{2}{C} i_b(K)\cdot t_{VM1}(K)\cdot K_{M1}(K) \\ &+ \frac{2}{C} i_c(K)\cdot t_{VS2}(K)\cdot K_{S2}(K)\end{aligned} \tag{20}$$

The dwell times of the selected virtual vectors are decided by the phase and amplitude of the reference vector. Therefore, the change rate of the NP potential is a function of the current vector, voltage vector and adjustment coefficient K as $\Delta v_{NP}(k) = f(I,V,K)$. When K=0, $\Delta v_{NP}(k) = f(I,V,0) = 0$ and the new virtual vectors return to conventional virtual vectors. This guarantees that there are no low-frequency oscillations of the NP. If a dc unbalance appears at a certain moment, it is preserved [25]. The NP dc unbalance can be recovered by adjusting K. Usually $I(k) \neq I(k+j)$ and $V(k) \neq V(k+j)$ so that the value of the adjustment factor directly affects the dynamic recovery process of the unbalanced NP potential. A hysteresis comparator and a proportional-integral controller are usually used to obtain an appropriate K in the dc unbalance state. The advantage of the hysteresis controller is simple and clear. The data of the NP potential is fed into the hysteresis comparator, then the controller determines whether the current value of K needs to change the value state. The final output value of K is 1 or -1 which is decided by the direction of the NP potential deviation. The main drawback of the hysteresis controller is the design of the ring width. In addition, only two values (1 or -1) of K affect the quality of the recovery process. A proportional-integral (PI) controller is better than a hysteresis loop. It can adjust the value of K continuously in a certain range. However, the PI controller also has its own shortcomings. It has one more parameter to be designed than the hysteresis controller. On the other hand, PI controllers work as a weak regulator for K adjustment, which manifests in two aspects: a) the input and output of the controller is a monotone function; b) in order to improve the unbalance recovery rate, K is set to the boundary value (1 or -1) at the start stage, and K can only be adjusted at the end stage. In summary, the two control methods are completely equivalent (since K=+1 or K=-1) before entering the end stage of the recovery process. However, since $I(k) \neq I(m)$ and $V(k) \neq V(m)$, there must be $\Delta v_{NP}(k) \neq \Delta v_{NP}(m)$ when K=1 or K=-1 at different sampling periods as shown in Fig. 13.

As a result, a six times the fundamental frequency oscillation of the NP voltage appears in the recovery process. Therefore, in consideration of the various control targets, a multi-objective optimization strategy based on the NP potential model is proposed in this paper, as shown in Fig. 14.

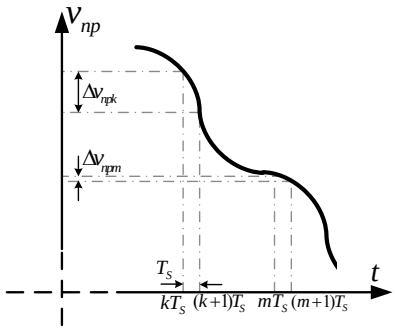

Fig. 13. Local recovery process of NP potential dc unbalance.

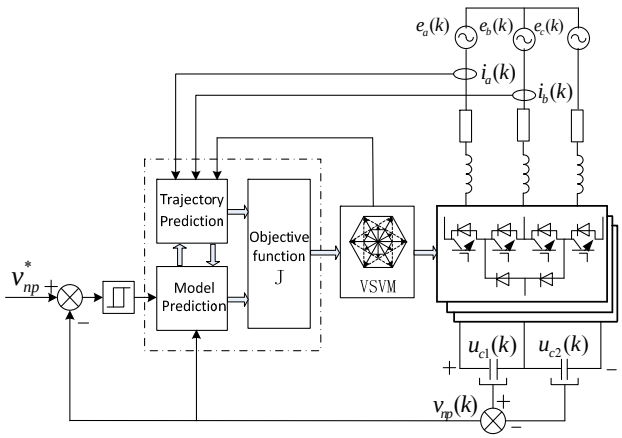

Fig. 14. Block diagram of Multi-objective optimization algorithm based on the NP voltage model.

The NP state of the three levels NPC converter in the next sampling interval can be predicted by Equ. (19), and the trajectory prediction module is applied to obtain $\Delta v_{NP}(k)$ by setting the regulator as the positive boundary in Equ. (20). Taking into account the six times frequency oscillation and the recovery speed, an objective function J to evaluate the performance of the adjusting factor K should be constructed. Finally the optimal value of K which makes J the minimum is used in the next sampling interval. This paper uses the normalized weighting method for transformation of multi-objective optimization, and the objective function J is as follows.

$$J = \left[v^*_{NP} - v_{NP}(k+1) \right]^2 + \lambda \cdot \left| v_{NP}(k) \right| \cdot \Delta v_{NP}(k)^2 \tag{21}$$

Here, λ is the weighted coefficient and v^*_{NP} is the ideal NP potential which is usually equal to zero. The objective function J contains two parts: a) $[v^*_{NP} - v_{NP}(k+1)]^2$ is the first part which is used to guarantee a faster recovery rate when making the minimum; b) the second one $\lambda \cdot v_{NP}(k) \cdot \Delta v_{NP}(k)^2$ reduces the oscillation and improves the quality of recovery process. Then the optimal K can be obtained by solving Equ. (21) as:

$$K = -\frac{1}{(\lambda + 1/|v_{NP}(k)|) \sum_{m=a,b,c} i_m(k) \cdot \dfrac{t_{m0\_\max}(k)}{T_S}} \cdot \mathrm{sgn}(v_{NP}(k))$$

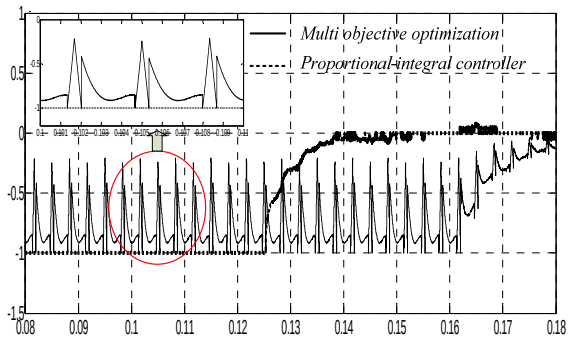

Fig. 15. Regulatory factor of two control strategies.

where $t_{m0\_\max}(k)$ is the action time of the NP current, when K is equal to the boundary value, and sgn(*) is a sign function.

The weighing factors λ handle the relation between the terms dedicated to the reference tracking, recovery rate, and six times frequency oscillation of the NP potential within J. A large value of a certain λ implies a greater priority to that objective. Equilibrium between the NP balancing speed and the quality (the size of six times the frequency oscillation) can be achieved through the proper configuration of λ. To measure the effect of the multi-objective optimization control strategy on the recovery speed and quality performance, it is important to define some of the performance variables. In the first place, the oscillating coefficient O_r is defined as the ratio of the minimum change rate of the NP potential and the maximum change rate in the recovery process of the NP potential dc unbalance. Thus:

$$O_r = \frac{\min(\Delta v_{NP}(k))}{\max(\Delta v_{NP}(k))}, k = 0,1,2\cdots,N \tag{22}$$

Where min (*) and max (*) are the minimum and maximum value functions, respectively. This makes it possible to measure or have an indication of the size of six times the frequency oscillation and the quality of the recovery process.

Fig. 15 shows the corresponding K of both the PI control and the multi-objective optimization control throughout the whole recovery process of the NP dc unbalance. The proposed multi-objective optimization control considers both the speed and oscillation of the recovery process. Therefore, the K value of this method varies in real-time.

V. Experimental Validation

To verify the effectiveness of the improved virtual vectors and multi-objective optimization control algorithm proposed in this paper, an experimental prototype is constructed as shown in Fig. 16.

The Experimental platform was based on a 380Vac, 100 A, 75 kVA, 3-L NPC converter, with SEMIKRON IGBT (SKiM301TMLI12E4B) switching at 5kHz. Each of the split capacitors has a capacitance value of 2.2 mF and the positive and negative dc link terminals of the inverter were supplied by a 600 V external rectifier unit, with the midpoint left

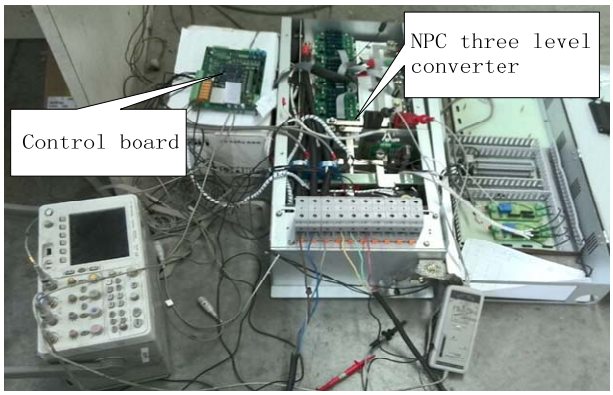

Fig. 16. Experiment equipment of NPC three-level converter.

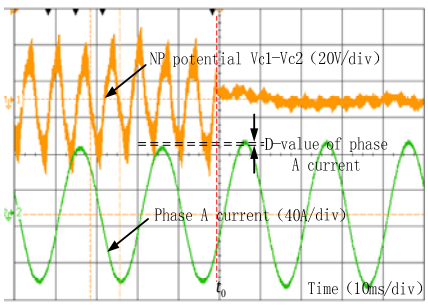

Fig. 17. Comparison of NPC three-level converter applying with NTV and NTV^2 modulation.

floating. A test for a NPC three-level converter working with the improved virtual vectors in the case of the NP potential without the dc unbalance was conducted. Fig.17 shows a comparison of the NP potential fluctuations between a NPC three-level converter using NTV modulation and NTV^2 modulation with the improved virtual vectors. When the modulation strategy is changed from NTV to NTV^2 at t0, the low frequency oscillation NP potential was successfully eliminated.

Due to the symmetry of the three-level NPC topology and the virtual space vector modulation, only the positive bias of the NP potential (voltage of C_1 is greater than C_2) is considered in this experiment. The results and conclusions under the state of the NP potential reverse bias are identical. Two different control strategies are conducted under the same conditions: the load is a resistor-inductance load, R = 4 ohms, L = 7.5mh, the modulation index is 0.95, the neutral point potential deviation of the initial state is 140v, and the bus voltage is 600v.

Fig.18 shows the whole recovery process of the NP potential dc unbalance based on the traditional virtual space vector modulation proposed in [9]. In Fig. 18(a) the NP potential control strategy began to work at the moment t1, and the unbalance of NP potential began to be suppressed. However, the recovery process of the unbalance was very slow and needed more than sixteen power cycles.

Fig. 18(b) clearly shows the local details of the purple shaded area in Fig.18(a). The blue shaded area in this figure

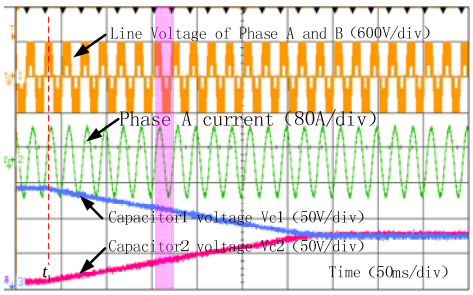

(a) Overall balance process.

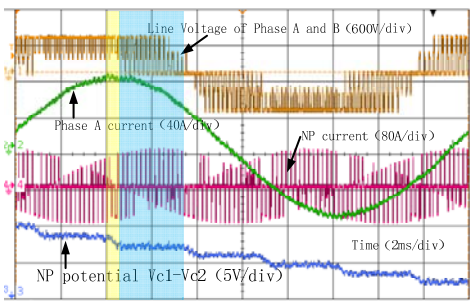

(b) Instantaneous part of balance process.

Fig. 18. Experimental result of conventional algorithm for NP balance under NTV^2 modulation.

means that the reference vectors are located in the A5 region of one sector, which represents the uncontrollable area of the NP potential in the traditional NTV^2 modulation in [9]. As can be seen from the blue shaded region in Fig. 18(b), the NP potential remained unchanged. The effective region, which can suppress the NP dc unbalance in the tradition NTV^2 modulation, is distributed in the small yellow shaded region. In addition, with the modulation index increasing, the blue shaded areas expand further, which means that the recovery rate is slower.

Fig. 19 shows the whole recovery process of the NP potential dc unbalance based on the improved virtual space vectors modulation with the multi-objective optimal control strategy. In Fig. 19(a) the NP potential control strategy began working at moment t1, and the unbalance of the NP potential began to be suppressed. The recovery process of the unbalance is much shorter and needs less than four power cycles. Fig. 19(b) clearly shows the local details of the purple shaded area in Fig. 19(a). As can be seen from Fig. 19(b), the deviation of the NP potential is always decreasing in both the yellow and blue shaded regions. In addition, the local recovery process is stable without major fluctuations.

To expose the possibilities of the proposed method, a graph showing the relationship between the design parameter λ and the recovery speed and quality is presented in Fig. 20.

From this figure, which is built based on several simulations for each value of λ, it is possible to confirm the above mentioned relation. Increasing λ implies a reduction in the size of six times the frequency oscillation and increases the time needed to restore the NP dc unbalance.

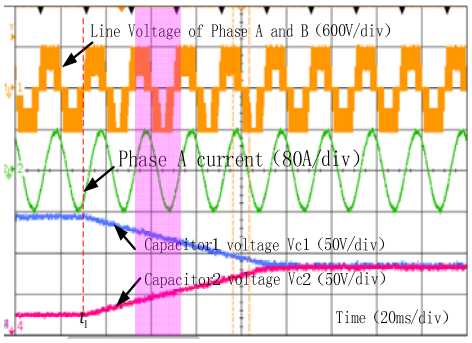

(a) Overall balance process.

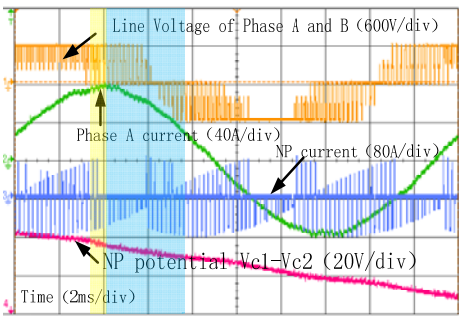

(b) Instantaneous part of balance process.

Fig. 19. Experimental results of Multi objective optimization algorithm for NP balance under NTV^2 modulation.

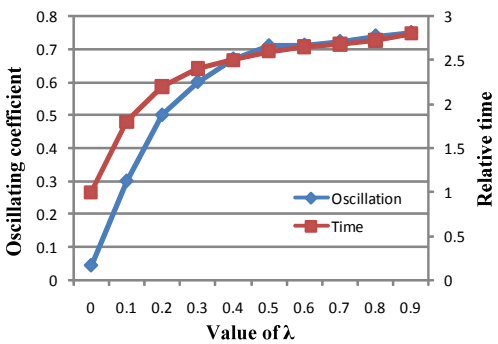

Fig. 20. Relation between the design parameter λ and the recovery speed and quality.

VI. Conclusions

This paper presented both the mechanism and equivalent model of the self-balancing for NPC converters under NTV and NTV^2 modulations. Although the NPC converter applied with NTV^2 modulation can easily eliminate low frequency oscillations, it barely has any self-balancing capacity unless there is a pure resistance load. That is to say, it hardly recoveries the NP unbalance without active controls. In older to improve the ability of recovering the NP dc unbalance for NPC converters applied with NTV^2 modulation, improved virtual space vectors and a multi objective optimization algorithm are proposed. The novel virtual space vectors put the whole SV plane under control without increasing the algorithm complexity. Furthermore, the multi objective optimization

algorithm makes use of an objective function *J* to obtain perfect equilibrium between the recovery speed and effect for the NP unbalance. The good performance of the proposed control has been verified through experimental results.

ACKNOWLEDGMENT

This work has been supported by the Fundamental Research Funds for the Central Universities under Award 2015XKMS030.

REFERENCES

[1] A. Nabae, I. Takahashi, and H. Akagi, "A new neutral-point clamped PWM inverter," *IEEE Trans. Ind. Applications.*, Vol. IA-17, No. 5, pp. 518-523, Sep. 1981.

[2] N. Celanovich and D. Boroyevich, "A comprehensive study of neutral point voltage balancing problem in three-level neutral-point-clamped voltage source PWM inverters," *IEEE Trans. Power Electron.*, Vol. 15, No. 2, pp. 242-249, Mar. 2000.

[3] H. du Toit Mouton, "Natural balancing of three-level neutral-point-clamped PWM inverters," *IEEE Trans. Ind. Electron.*, Vol. 49, No. 5, pp. 1017–1025, Oct. 2002.

[4] R. Sommer, A. Mertens, C. Brunotte, and G. Trauth, "Medium voltage drive system with NPC three-level inverter using IGBTs," *PWM Medium Voltage Drives (Ref. No. 2000/063) IEE Seminar*, pp. 3/1–3/5, 2000.

[5] R.W. Menzies, P. Steimer, J. K. Steinke, "Five-level GTO inverters for large induction motor drives," *IEEE Trans. Ind. Appl.*, Vol. 30, No. 4, pp. 938-944, Jul./Aug. 1994.

[6] J. Pou, R. Pindado, D. Boroyevich, and P. Rodriguez, "Limits of the neutral-point balance in back-to-back-connected three-level converters," *IEEE Trans. Power Electron.*, Vol. 19, No. 3, pp. 722-731, May 2004.

[7] C. Xia, X. Gu, T. Shi, and Y. Yan, "Neutral-point potential balancing of three-level inverters in direct-driven wind energy conversion system," *IEEE Trans. Energy Convers.*, Vol. 26, No. 1, pp. 18-29, Sep. 2010.

[8] C. Xia, H. Shao, Y. Zhang, and X. He, "Adjustable proportional hybrid SVPWM strategy for neutral-point-clamped three-level inverters," *IEEE Trans. Ind. Electron.*, Vol. 60, No.10, pp. 4234-4242, Aug. 2012.

[9] J. Pou, P. Rodriguez, V. Sala, S. Busquets-Monge, and D. Boroyevich, "Algorithm for the virtual vectors modulation in three-level inverters with a voltage-balance control loop," in *Conference on Power Electronics and Applications*, pp. P.1-P.9, 2005.

[10] S. Busquets-Monge, J. Bordonau, D. Boroyevich, and S. Somavilla, "The nearest three virtual space vector PWM - a modulation for the comprehensive neutral-point balancing in the three-level NPC inverter," *IEEE Power Electron. Lett.*, Vol. 2, No.1, pp. 11-15, Mar. 2004.

[11] J. Pou, D. Boroyevich, and R. Pindado, "New feed forward space-vector PWM method to obtain balanced AC output voltages in a three-level neutral-point-clamped converter," *IEEE Trans. Ind. Electron.*, Vol. 49, No. 5, pp. 1026-1034, Oct. 2012.

[12] J. Shen, S. Schröder, R. Rösner, and S. El-Barbari, "A comprehensive study of neutral-point self-balancing effect in neutral-point-clamped three-level inverters," *IEEE Trans. Power Electron.*, Vol. 26, No. 11, pp. 3084-3095, Nov. 2011.

[13] P. Szczepankowski and J. Nieznanski, "Virtual space vector pulse width modulation algorithm for three-level NPC converters based on the final element shape functions," in *Conference on Industrial Electronics Society(IECON)*, pp.3824-3829, 2013.

[14] S. Busquets-Monge, J. D. Ortega, J. Bordonau, J. A. Beristain, and J. Rocabert, "Closed-loop control of a three-phase neutral-point-clamped inverter using an optimized virtual-vector-based pulse width modulation," *IEEE Trans. Ind. Electron.*, Vol. 55, No. 5, pp. 2061-2071, May 2008.

[15] J. Zaragoza, J. Pou, S. Ceballos, E. Robles, C. Jaen, and M. Corbalan, "Voltage-balance compensator for a carrier-based modulation in the neutral-point-clamped converter," *IEEE Trans. Ind. Electron.*, Vol. 56, No. 2, pp. 305-314, Nov. 2008.

[16] J. Pou, J. Zaragoza, P. Rodriguez, S. Ceballos, V.M. Sala,R. P. Burgos, and D. Boroyevich, "Fast-processing modulation strategy for the neutral-point-clamped converter with total elimination of low-frequency voltage oscillations in the neutral point," *IEEE Trans. Ind. Electron.*, Vol. 54, No. 4, pp. 2288-2294, Aug. 2007.

[17] Z. Ye, F. Li, Y. Xu, X. Deng, and Y. Zhang, "Simplified PWM strategy for neutral-point-clamped (NPC) three-level converter," *Journal of Power Electronics*, Vol 14, No 3, pp 519-530, Mar. 2014.

[18] K. S. Amitkumar and G. Narayanan, "Simplified implementation of space vector PWM strategies for a three level inverter," in *Conference on Industrial and Information Systems (ICIIS)*, pp. 1-6, 2012.

[19] A. H. Bhat and N. Langer, "Capacitor voltage balancing of three-phase neutral-point-clamped rectifier using modified reference vector," *IEEE Trans. Power Electron.*, Vol. 29, No. 2, pp. 561-568, Apr. 2013.

[20] S. Fukuda and Y. Matsumoto, "Optimal-regulator-based control of NPC boost rectifiers for unity power factor and reduced neutral point potential variations," *IEEE Trans. Ind. Electron.*, Vol. 46, No. 3, pp. 527-534, Jun. 1999.

[21] T. Ito, M. Kamaga, Y. Sato, and H. Ohashi, "An investigation of voltage balancing circuit for DC capacitors in diode-clamped multilevel inverters to realize high output power density converters," in *Conference on Energy Conversion Congress and Exposition (ECCE)*, pp. 3675-3682, 2010.

[22] F. B. Grigoletto and H. Pinheiro, "Generalized pulse width modulation approach for DC capacitor voltage balancing in diode clamped multilevel converters," *IET Power Electron.*, Vol. 4, No. 1, pp. 89-100, Jan. 2011.

[23] J. Holtz and N. Oikonomou, "Neutral point potential balancing algorithm at low modulation index for three-level inverter medium voltage drives," *IEEE Trans. Ind. Appl.*, Vol. 43, No. 3, pp. 761-768, May 2007.

[24] J.-H. Seo, C.-H. Choi, D.-S. Hyun, "A new simplified space-vector PWM method for three-level inverters," *IEEE Trans. Power Electron.*, Vol. 16, No. 4, pp. 545-550, Jul. 2001.

[25] S. Busquets-Monge, S. Somavilla, J. Bordonau, and D. Boroyevich, "Capacitor voltage balance for the neutral-point- clamped converter using the virtual space vector concept with optimized spectral performance," *IEEE Trans. Power Electron.*, Vol. 22, No. 4, pp. 1128-1135, Jul. 2007.

Chuan-Jin Zhang was born in Xuzhou, China, in 1986. He received his B.S. degree from the School of Electrical Engineering, Northeast Dianli University, Jilin, China, in 2009; and his M.S. degree in Power Electronics and Drives from the China University of Mining and Technology, Xuzhou, China, in 2012; where he is presently working towards his Ph.D. degree in the School of Information and Electrical Engineering. His current research interests include power quality compensation systems, motor control and power electronics.

Yi Tang was born in Zhangjiagang, China, in 1957. He received his Ph.D. degree from the School of Information and Electrical Engineering, China University of Mining and Technology, Xuzhou, China, in 1995. He is presently working as a Professor in the China University of Mining and Technology. His current research interests include power quality and power system analysis.

Dong Han was born in Xuzhou, China, in 1991. He received his B.S. degree in Electrical Engineering and Automation from the Jin Ling Institute of Technology, Nanjing, China, in 2013. He is presently working toward his M.S. degree in Electrical Engineering from the China University of Mining and Technology, Xuzhou, China. His current research interests include power quality and multilevel inverters.

Hui Zhang was born in Xuzhou, China, in October 1983. He received his B.S. degree in Electrical Engineering and his Ph.D. degree in Power Electronics and Electrical Drives from the China University of Mining and Technology, Xuzhou, China, in 2006 and 2011, respectively. In 2012, he became a Lecturer in the School of Information and Electrical Engineering, China University of Mining and Technology. His current research interests include power quality, motor control and power electronics.

Xiao Zhang was born in Baoji, China, in 1974. He received his M.S. and Ph.D. degrees from the School of Information and Electrical Engineering, China University of Mining and Technology, Xuzhou, China, in 2003 and 2012, respectively. In 1997, he joined the China University of Mining and Technology as a Teaching Assistant, where he has been an Associate Professor, since 2009. From October 2013 to October 2014, he was a Visiting Professor at Ohio State University, Columbus, OH, USA. His current research interests include power electronic converters, reactive power control, harmonics, power quality compensation systems, and the application of power electronics in renewable energy systems and motor control.

Ke Wang was born in Xuzhou, China, in 1985. He received his B.S. degree in Electrical Engineering and Automation and his M.S. degree in Power Electronics and Drives from the China University of Mining and Technology, Xuzhou, China, in 2005 and 2009, respectively; where he is presently working towards his Ph.D. degree in the School of Information and Electrical Engineering. His current research interests include power electronic converters, active power filters and fault diagnosis.